revised manuscript, submitted to *Geophys. J. Int.* version: 2020-02-05 compiled: May 28, 2020

A single Rayleigh mode may exist with multiple values of phase-velocity at one frequency

Thomas Forbriger[1], Lingli Gao[2], Peter Malischewsky[3], Matthias Ohrnberger[4], Yudi Pan[5]

[1] *Karlsruhe Institute of Technology (KIT), Geophysical Institute, Black Forest Observatory (BFO), Heubach 206, 77709 Wolfach, Germany, E-mail: Thomas.Forbriger@kit.edu*

[2] *Institute of Applied and Numerical Mathematics, Karlsruhe Institute of Technology (KIT).*

[3] *Institute of Geosciences, Friedrich-Schiller University Jena*

[4] *Institute of Earth and Environmental Sciences, University of Potsdam*

[5] *Geophysical Institute, Karlsruhe Institute of Technology (KIT)*

May 28, 2020

SUMMARY

Other than commonly assumed in seismology, the phase velocity of Rayleigh waves is not necessarily a single-valued function of frequency. In fact, a single Rayleigh mode can exist with three different values of phase velocity at one frequency. We demonstrate this for the first higher mode on a realistic shallow seismic structure of a homogeneous layer of unconsolidated sediments on top of a half-space of solid rock (LOH). In the case of LOH a significant contrast to the half-space is required to produce the phenomenon. In a simpler structure of a homogeneous layer with fixed (rigid) bottom (LFB) the phenomenon exists for values of Poisson's ratio between 0.19 and 0.5 and is most pronounced for P-wave velocity being three times S-wave velocity (Poisson's ratio of 0.4375). A pavement-like structure (PAV) of two layers on top of a half-space produces the multi-valuedness for the fundamental mode.

Programs for the computation of synthetic dispersion curves are prone to trouble in such cases. Many of them use *mode-follower* algorithms which loose track of the dispersion curve and miss the multi-valued section. We show results for well established programs. Their inability to properly handle these cases might be one reason why the phenomenon of multi-valuedness went unnoticed in seismological Rayleigh wave research for so long.

For the very same reason methods of dispersion analysis must fail if they imply wave number $k_l(\omega)$ for the l-th Rayleigh mode to be a single-valued function of frequency ω. This applies in particular to deconvolution methods like phase-matched filters. We demonstrate that a slant-stack analysis fails in the multi-valued section, while a Fourier-Bessel transformation captures the complete Rayleigh-wave signal.

Waves of finite bandwidth in the multi-valued section propagate with positive group-velocity and negative phase-velocity. Their eigenfunctions appear conventional and contain no conspicuous feature.

Key words: Surface waves and free oscillations, Theoretical seismology, Wave propagation

1 INTRODUCTION

1.1 Statement of the problem

Rayleigh waves are used in tele-seismic studies (Kovach 1978; Kästle *et al.* 2018, e. g.) as well as in shallow seismics (Socco *et al.* 2010; Foti *et al.* 2018, e. g.) to investigate Earth's structure. On a stratified half-space the propagation velocity of these waves depends on frequency, i. e. they are dispersive. The dispersion relation carries information on subsurface properties. In particular the shear-wave velocity structure controls how Rayleigh-wave velocity relates to frequency. Commonly used algorithms inherently expect the relation of phase velocity $c(f)$ to frequency f to be a single-valued function. For Lamb-waves (Lamb 1917), a particular type of Rayleigh waves in isolated plates, which are used in engineering to study mechanical properties of constructional elements, this is not generally the case. This fact is well known in fields of ultrasonic and structural engineering. That this phenomenon also exists for seismic waves in layered structures on an elastic half-space or with a rigid bottom to our knowledge went unnoticed in seismology until recently (Malischewsky *et al.* 2017). We investigate the properties of wave fields with multi-valued dispersion relation for Rayleigh modes and the applicability of common methods in surface wave seismology.

1.2 Reported cases from engineering

We refer to the detailed review of literature provided by Cui *et al.* (2016) in their introduction. They describe studies of elastic waves in bodies of different geometry (plates, rods, etc), both theoretical investigations as well as experimental confirmation. The phenomenon is frequently referred to as 'backward wave propagation', or 'negative group velocity' (NGV) (Negishi 1987, e. g.) and is discussed as occurrence of 'zero group velocity' (ZGV) (Kausel 2012, e. g.). We will discuss this nomenclature below. Similar phenomena of 'negative refraction' are reported for electromagnetic wave propagation (Oulton & Pendry 2013; Pendry 2009).

Almost all reported studies of elastic materials use isolated bodies like rods, pipes, or thin plates with two free surfaces. In contrast Maznev and Every (2011; 2009) discuss the existence of this phenomenon for thin layers on a substrate. They study surface acoustic waves in a thin film structure on silicon. The surface waves in these structures, with one free surface only, hence are similar to seismic Rayleigh waves. Every (2002) and Cès *et al.* (2011) describe measurements on supported structures. Maznev and Every (2011) discuss the 'clamped-free layer' (which we call 'layer with fixed bottom', *LFB*), the 'layer on elastic substrate' (which we call 'layer on half-space', *LOH*), and the 'bi-layer structure' (which we call 'pavement structure', *PAV*). They suppose that the phenomenon went unnoticed for such a long time, because a significant contrast in elastic properties between layer and substratum is required for its existence. The phenomenon depends on Poisson's ratio ν and is strongest for $\nu = \sqrt{7/16} = 0.4375$, where P-wave velocity is three times S-wave velocity, a value reported also by Malischewsky *et al.* (2017). Maznev and Every (2011) go beyond normal modes and discuss leaky modes as well. The phenomenon exists in combination with osculation points of dispersion curves (Kausel *et al.* 2015) and according to Maznev and Every (2011) can be partly understood by consideration of mode degeneracy and hybridization.

1.3 Multi-valued dispersion in seismic structures

Malischewsky *et al.* (2017) and Malischewsky and Forbriger (2020) report that the condition of a single-valued dispersion relation can as well be violated for simple seismic structures of a layer on top of a half-space. To our knowledge, these are the only explicit reports on this phenomenon in the seismological literature so far. In ignorance of the phenomenon common algorithms were designed in a way to implicitly require single-valuedness of the dispersion relation. Consequently the phenomenon cannot be discovered when using these particular algorithms.

The problem might also have been missed because it requires a strong vertical contrast in seismic velocities and values of Poisson's ratio, which are not present in the deeper crust or upper mantle. The required velocity-contrast and range of Poisson's ratio however can exist in shallow seismic structures (Forbriger 2003b, sec. 2.5.1) and basins like the Mexico City valley (Malischewsky *et al.* 2017).

The phenomenon is strongest for structures with a rigid bottom. Tuan (2009, Figure 2.6) presents multi-valued dispersion curves of phase velocity for a gradient layer with fixed bottom. However, he neither mentions the phenomenon in the text nor in the figure caption. Below we use a structure of a homogeneous layer with fixed bottom (LFB) to discuss properties of propagating waves.

The investigation by Lysmer (1970) is the only example we are aware of where negative group velocity is reported for a seismic structure (with rigid bottom instead of a free plate) published in a seismological journal. Lysmer studies layered structures with a rigid base, where the rigid bottom may be at quasi infinite depth. He reports negative values of group velocity (Lysmer 1970, Table 4) for an LFB case, which is a clear indication of the phenomenon of a multi-valued relation between phase-velocity and frequency. However, he presents frequency as a function of wave number (Lysmer 1970, Figure 5) and phase-velocity as a function of wave number (Lysmer 1970, Figure 6), which both are single-valued relations. If direction of propagation would be defined with respect to the location of a source, group-velocity will turn positive and phase-velocity will become negative, as explained below in section 4.1.

1.4 Structure of this contribution

In the current contribution we show examples of multi-valued Rayleigh wave dispersion in shallow seismic structures, investigate the nature of wave propagation in the frequency band of multi-valuedness, and point out consequences for practical application of common methods and ways to mitigate detriments. We first introduce the phenomenon by a simple example of a single layer on top of a half-space (*LOH*). In that case the first higher Rayleigh mode can develop a multi-valued section of the dispersion relation. Next we point out the consequences a multi-valuedness can have. Most importantly, the application of conventional techniques for the computation of dispersion curves or the analysis of recorded Rayleigh waves can produce false results. Because the discussed type of dispersion characteristic is so unfamiliar, we then investigate the properties of the Rayleigh modes in terms of their eigenfunctions, their group velocity, and the nature of the resulting propagating wave-trains. We find no conspicuous feature in the eigenfunctions but can demonstrate that waves actually propagate with negative phase-velocity and as a consequence are missed in slant stack analyses of dispersive waves. As a closing remark, we demonstrate that the dispersion relation of the fundamental Rayleigh mode can be multi-valued for pavement-like structures.

2 THE PHENOMENON OF MULTI-VALUED DISPERSION RELATION

2.1 Normal modes

To provide a proper definition of quantities displayed in the various figures, we briefly introduce the fundamental concepts of normal modes. Normal modes exist for solutions of the homogeneous elastic vector differential equation which satisfy the boundary condition of a stress-free surface at $z = 0$ and do not radiate energy into the half-space. These conditions are satisfied at the roots of the characteristic function $\Delta_{\mathrm{R}}(f, p)$ (Takeuchi & Saito 1972, eq. 66). Hence normal modes exist for pairs of frequency f and phase slowness p where the 'secular equation'

$$\Delta_{\mathrm{R}}(f, p) = 0 \tag{1}$$

is satisfied. This is an implicit definition of the dispersion relation. Phase slowness p may as well be substituted by phase velocity $c = p^{-1}$ or wave number $k = p\,\omega$ with $\omega = 2\pi\, f$. The characteristic function is derived from the determinant of a matrix (Aki & Richards 2002, eq. 7.59) which sometimes is called the 'Rayleigh determinant'. Malischewsky *et al.* (2017, eq. 1) give the characteristic function for a homogeneous layer with fixed bottom (*LFB*) in closed form. It is composed of products of nested transcendental functions. They result from the expressions which govern the

Table 1. Model *LOH* (layer over half-space). Seismic parameters are chosen such that they are realistic for shallow seismic structures. Reasonable ranges are discussed by Forbriger (2003b, sec. 2.5.1). j: layer index, z_j: depth to bottom of layer, $v_{\mathrm{P}j}$, $v_{\mathrm{S}j}$: velocity of compressional and shear waves, ν_j: Poisson's ratio, ρ_j: mass density. $j = 2$ for the elastic half-space. To provide anelastic dissipation in the computation of Fourier-Bessel expansion coefficients quality is set to $Q_\mathrm{P} = Q_\mathrm{S} = 100$.

j	z_j/m	$v_{\mathrm{P}j}$/m s^{-1}	$v_{\mathrm{S}j}$/m s^{-1}	ν_j	ρ_j/kg m^{-3}
1	2	532.8	177.6	0.4375	1800
2	∞	4000.0	2310.0	0.2498	2600

eigenfunctions of the mode. For a structure of a homogeneous layer on top of a homogeneous half-space (*LOH*) the characteristic function is significantly more complex. Tuan (2009, eq. 3.10) presents it in closed form with nested expressions for the coefficients.

From the range of values for compressional- and shear-wave velocity in the structure results a range of phase velocity and phase slowness, respectively, in which normal modes can exist. In a layered structure at each phase velocity (or phase slowness, respectively) in this range there exists an infinite number of discrete normal modes, which are called the fundamental mode (at smallest frequency) and overtones (or higher modes).

In a stratified half-space the roots of the characteristic function appear along continuous curves. It hence appears natural to express the dispersion relation in terms of one function for each mode relating frequency to phase slowness. In the current contribution we demonstrate that these continuous relations not necessarily are single-valued functions. They rather can be multi-valued in that for a single mode there may exist several values of phase slowness at one frequency.

Due to reasons of symmetry the direction of wave propagation along the surface does not affect wave velocity on a layered structure. Hence identical modes exist for positive as well as the corresponding negative values of phase velocity (or phase slowness, respectively). The sign of velocity with respect to spatial coordinates only comes into play if a source of energy is explicitly defined. This is commonly neglected in surface wave theory and only positive values of phase velocity (or phase slowness, respectively) are discussed. Their negative counterparts do not add information regarding the problem of surface wave dispersion. Only in Fig. 1 we display both signs. In all other figures the symmetry is understood implicitly.

At each frequency there can exist Rayleigh waves with several different values of phase-slowness. This is because of 1) the existence of multiple modes (overtones), 2) the continuous dispersion relation of each mode appearing at several values of phase-slowness for the same frequency, and 3) the sign of phase-slowness indicating different direction of propagation. The different values of phase-slowness are not alternatives to each other. Rayleigh waves may exist at all these values at once, their level of excitation being controlled by the actual seismic source. In the current contribution we specifically discuss cases multi-valued dispersion relation where multiple values of phase-slowness may appear along the continuous dispersion relation at one single frequency. Occasionally we refer to the phenomenon of 'multi-valued dispersion relation' as 'reversal of the dispersion curve'.

2.2 Layer on top of an elastic half-space (*LOH*)

To demonstrate the phenomenon of a multi-valued dispersion relation, we use a simple structure of a homogeneous, elastic layer on top of a homogeneous, elastic half-space (*LOH*). Parameters of this structure are given in Table 1. Values are in the typical range of a 2 m thick layer of unconsolidated sediments on top of a half-space of solid rock (Forbriger 2003b, sec. 2.5.1). We use an algorithm by Schwab & Knopoff (1972) to compute the characteristic function $\Delta_\mathrm{R}(f,p)$ for this structure as a function of frequency f and phase slowness p. Buchen & Ben-Hador (1996, eq. 13) provide an excellent review of the theoretical background of established equivalent algorithms for the numerical computation of the characteristic function for layered structures.

Fig. 1 displays the sign-pattern of the characteristic function.

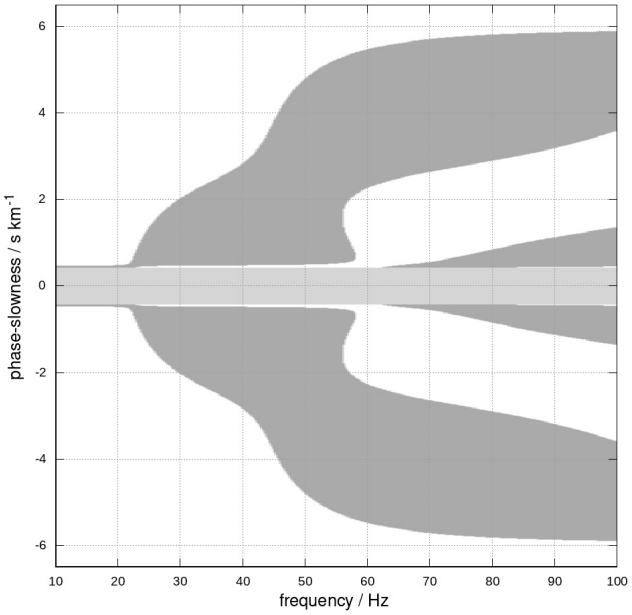

Figure 1. Sign of the characteristic function $\Delta_\mathrm{R}(f,p)$ for model *LOH* (Table 1). Grey and white areas have opposite sign. The function is symmetric with respect to p and $\Delta_\mathrm{R}(f,p) = \Delta_\mathrm{R}(f,-p)$. Normal modes exist where the secular equation $\Delta_\mathrm{R}(f,p) = 0$ is satisfied, i. e. along the lines where areas of different colors touch. Normal modes do not exist in the light-gray area at phase slowness $|p| < v^{-1}_{\mathrm{S,halfspace}}$, because energy would be radiated into the half-space. Usually only solutions for $p > 0$ are considered. The direction of propagation and hence the sign of p is meaningless unless a source location is defined.

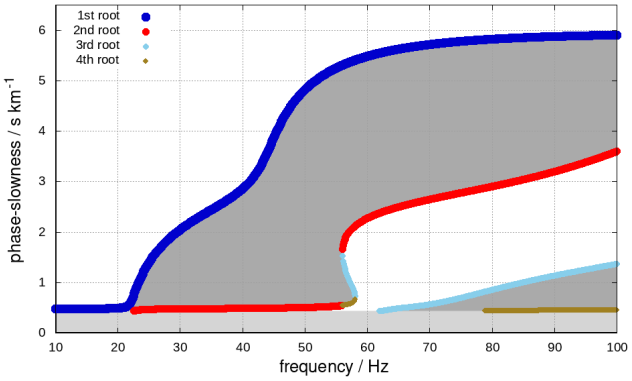

Figure 2. Roots of the characteristic function $\Delta_\mathrm{R}(f,p)$ for model *LOH* (Table 1, Fig. 1). At each frequency f the roots $\Delta_\mathrm{R}(f,p) = 0$ are searched and counted in order of decreasing phase-slowness p. They are marked by colored dots, which are placed very densely.

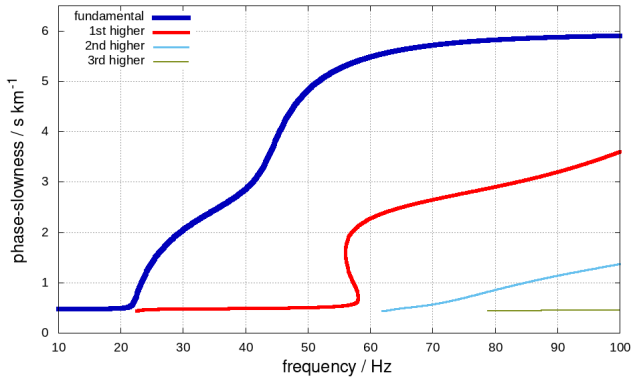

Figure 3. Dispersion curves of Rayleigh normal modes for model *LOH*. The roots of the characteristic function (Fig. 2) are assigned to the fundamental mode and overtones. They are aligned along continues curves, which mark the dispersion relation of the respective mode. The relation between phase slowness and frequency for the first higher mode is a multi-valued function between 56 Hz and 58 Hz. Fig. 2 clearly indicates that three different values of phase slowness exist for the first higher mode at each frequency in this interval.

Positive values are white, negative values are gray (or vice versa, the characteristic function is defined except for a constant factor). In the light gray area for $|p| < v_{\mathrm{S,halfspace}}^{-1}$, with $v_{\mathrm{S,halfspace}} = v_{\mathrm{S}2}$ in Table 1, there exist no normal modes because the lower boundary condition cannot be satisfied, i. e. shear waves would be radiated into the half-space. Normal modes exist at the contact between white and gray areas. These are the locations of the roots of the characteristic function which satisfy the secular equation $\Delta_{\mathrm{R}}(f,p) = 0$. The pattern is symmetric with respect to $p = 0$, because the direction of propagation is meaningless for the existence of normal modes as pointed out in the previous section. Because solutions at $p < 0$ do not add independent information, all considerations usually are limited to positive values of p. Nevertheless we

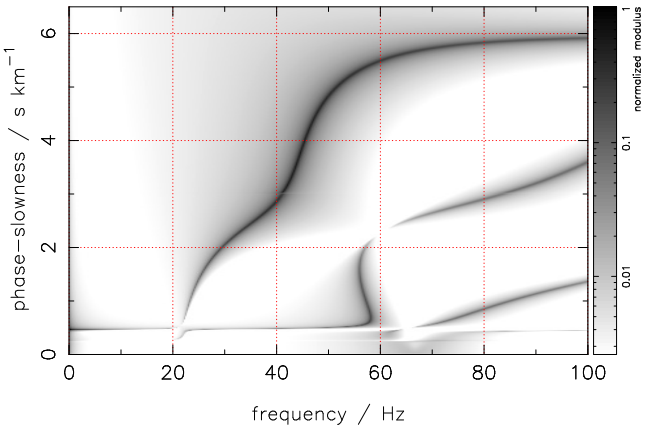

Figure 4. Modulus of Fourier-Bessel expansion coefficients for vertical displacement and a vertical single force acting on the surface of structure *LOH* (Table 1). See appendix A for a definition. Large amplitudes (dark gray to black) indicate Rayleigh-wave signals along the dispersion curves (see Fig. 3). This is displayed for independent confirmation of the reversal of the dispersion curve for the first higher mode in the frequency interval between 56 Hz and 58 Hz. Signals at phase slowness $p < v_{\mathrm{S,halfspace}}^{-1} \approx 0.433\,\mathrm{s\,km^{-1}}$ with $v_{\mathrm{S,halfspace}} = v_{\mathrm{S}2}$ in Table 1 formally are not attributed to the normal modes. They radiate energy into the half-space. From the perspective of propagating waves they hardly differ from Rayleigh waves.

shall keep in mind that the corresponding solutions at negative p still exist. Below we will refer to this in the discussion of a wave field excited by an actual source.

Searching for zero-crossings of $\Delta_{\mathrm{R}}(f,p)$ at each frequency f parallel to the the p-axis we locate the roots. They are marked by densely placed dots in Fig. 2. Roots of $\Delta_{\mathrm{R}}(f,p)$ exist along continuous lines, the so-called 'dispersion curves' (Fig. 3).

2.3 Multi-valued dispersion relation

It is obvious in Fig. 3 that the dispersion relation $p(f)$ of the first higher mode is multi-valued in the frequency band from 56 Hz to 58 Hz. Strictly, the dispersion relation no longer may be expressed by a function $p(f)$ which would imply a single-valued relation. The dispersion better should be expressed by the implicit definition $\Delta_{\mathrm{R}}(f,p) = 0$. In this band there exist three different values of phase slowness at each single frequency. Because phase velocity $c = p^{-1}$ and wave number $k = 2\pi f p$ are just scaled versions of phase slowness p, the situation is not different if dispersion is expressed as $c(f)$ or $k(\omega) = k(2\pi f)$.

In seismology and applied seismics the possibility of a multi-valued dispersion relation usually is ignored on purpose. We are not aware of any literature in these fields mentioning the possibility of this phenomenon.

As an independent proof of the existence of this phenomenon, we display the modulus of Fourier-Bessel expansion coefficients (see appendix A) for the waves generated by a single vertical force (like a hammer blow) on the structure defined in Table 1. The large amplitudes, which are apparent in Fig. 4 by dark gray regions, compose the Rayleigh waves. They are located along the dispersion curves as displayed in Fig. 3 including the section of reversal of the dispersion curve. The characteristic function appears in the denominator of the expression for the Fourier-Bessel expansion coefficients as pointed out by Kennett and Kerry (1979, section 5.4) and Müller (1985, eqs. 83 and 86). This would cause singularities along the dispersion curves. No singularities appear here, because the roots are slightly shifted away from the real slowness-axis due to finite Q-values in the seismic parameters (Müller 1985, section 4.3). The roots of the characteristic function in the denominator still result in a large magnitude of the expansion coefficients along the dispersion curves.

3 FALSE RESULTS DUE TO THE PHENOMENON

3.1 Computation of synthetic dispersion curves fails

Commonly used programs for the computation of synthetic dispersion curves use sophisticated algorithms like 'root-followers' and 'root-count' (Woodhouse 1988), other than we do by locating all roots at each single frequency (Fig. 2). These programs estimate the asymptotic phase-slowness at a large frequency (where only the topmost layer controls surface wave propagation). They identify one of the roots as the desired overtone at this frequency and then compute the dispersion relation by following this root to smaller frequencies. In the case of a multi-valued dispersion relation these algorithms loose track of the root at the next smaller frequency when the curve actually turns to increasing frequency. They miss the reversal of the curve. In Fig. 5 we demonstrate this for the dispersion curves given by `geopsy` (Geopsy team 2017; Wathelet *et al.* 2004; Wathelet 2008). The root-follower looses track at about 56 Hz. It continues the search for roots of the current overtone with

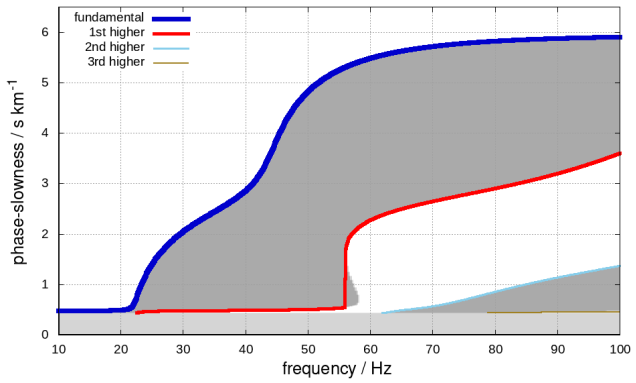

Figure 5. Dispersion curves computed by `geopsy` for model *LOH* (Table 1). The so-called 'root-follower' misses part of the dispersion of the first higher mode in the frequency interval between 56 Hz and 58 Hz.

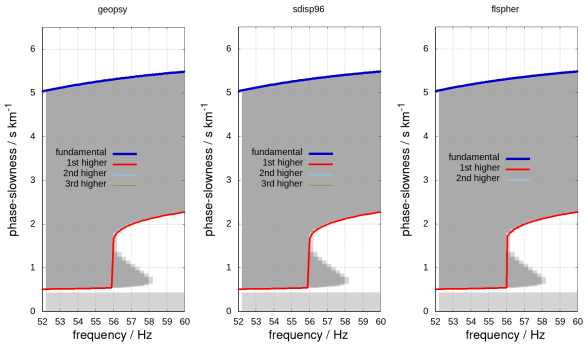

Figure 6. Dispersion curves computed by three different programs. Left: `geopsy`. Middle: `sdisp96` (Computer Programs in Seismology). Right: `flspher`. See text for references. All miss part of the dispersion of the first higher mode in the frequency interval between 56 Hz and 58 Hz.

strictly decreasing frequency. In consequence it misses part of the dispersion relation in the frequency interval in which it is multi-valued. Surprisingly these algorithms are rarely discussed in literature. Their purpose seems to be too trivial.

We test three different well established programs for the computation of dispersion curves. They are all able to properly compute the characteristic function and its roots. Their root-followers however fail to capture the complete dispersion relation in the frequency interval where it is multi-valued. We compare their results in Fig. 6. Next to the results by `geopsy` (Geopsy team 2017; Wathelet *et al.* 2004; Wathelet 2008), which are also shown in Fig. 5, we display the output of `sdisp96` (Herrmann 2013, Computer Programs in Seismology) and `flspher`. The latter is based on an algorithm by Friederich (1999; 1995) modified for shallow seismics. All three miss the multi-valued section in the above mentioned way.

The common property of many established programs to miss the multi-valued section might be a reason, why this phenomenon went unnoticed in seismology and applied seismics for such a long time. Researchers were simply not able to detect the phenomenon in computation of synthetic dispersion curves, because the computed relation $p(f)$ in all cases is single-valued by design.

3.2 Methods of dispersion analysis fail

Surface wave dispersion commonly is expressed as a function of frequency (rather than frequency as a function of wave number), because the first step in dispersion analysis of recorded seismograms is a Fourier transformation. Analysis algorithms then derive the dispersion relation from the difference in Fourier phase of signals at different offset to the source. There is only one value of Fourier phase at each frequency. In cases where multiple overtones interfere in the seismogram, phase-matched filter techniques can be used to isolate a single mode in the waveform signal (Herrin & Goforth 1977; Russell *et al.* 1988; Sèbe *et al.* 2009). These techniques essentially apply a deconvolution with a reference dispersion $p_{\mathrm{ref}}(f)$ in order to concentrate the seismic energy of the respective mode in a small time window. Again there is no room for more than one value of $p_{\mathrm{ref}}(f)$ at each frequency f. Even the simple, robust and widely-used approach of a slant-stack for dispersion analysis of multi-channel data (McMechan & Yedlin 1981; Gabriels *et al.* 1987; Forbriger 2003a) is likely to fail in the case of the discussed phenomenon. We demonstrate this below.

4 RAYLEIGH MODE PROPERTIES

4.1 Group slowness

The reported reversal of the dispersion curve for phase velocity goes along with group velocity apparently becoming negative in the frequency band of multi-valuedness of the dispersion relation. Malischewsky and Forbriger (2020) discuss this for the case of the valley of Mexico City. Appendix B summarizes the well known relation between phase- and group-slowness dispersion. At 57 Hz in Fig. 3 phase slowness decreases with frequency at a rate of

$$\frac{\mathrm{d}\,p(f)}{\mathrm{d}\,f} \approx -0.32\,\frac{\mathrm{s}^2}{\mathrm{km}} < -\frac{1.071}{57}\,\frac{\mathrm{s}^2}{\mathrm{km}} = -0.019\,\frac{\mathrm{s}^2}{\mathrm{km}}. \qquad (2)$$

This corresponds to a negative group-slowness according to eq. (B.16) in appendix B.

This is common to many cases of multi-valued dispersion reported in literature. Hence 'negative group-velocity' is a term frequently used to name this phenomenon and has made it into the title of several papers (Negishi 1987; Wolf *et al.* 1988; Tamm *et al.* 2017; Nishimiya *et al.* 2007). This term is misleading and might appear like a violation of accepted physics, where group velocity in non-dissipative media equals velocity of energy transport (Carcione *et al.* 2010). Energy certainly always emerges from the source and propagates away from the source, the direction which usually is defined as positive. It only seems there is a conflict here. This is because no source is defined in normal mode theory. What is meant by 'negative group-velocity' hence is synonymous with 'phase-velocity and group-velocity have opposite sign' in this case. In fact, Lamb (1904) in his contribution, which is frequently cited in the context of 'negative group-velocity', explicitly states that group velocity always is in direction away from the source. In a coordinate system defined with respect to the source it always will be positive, while phase velocity might become negative. In their discussion of the dispersion of Lamb-waves Tolstoy and Usdin (1957) emphasize that group velocity never should be taken negative.

Nevertheless we study the physical properties of the Rayleigh mode in the multi-valued frequency band. The variation of amplitude with depth is defined by the so-called eigenfunctions of normal mode theory. Properties of actual wave propagation of a signal of finite bandwidth (including group slowness) are studied by computing synthetic seismograms.

4.2 Eigenfunctions

Fig. 7 displays eigenfunctions for the displacement components of the first overtone in the multi-valued section of the dispersion curve. The panels start at small frequency and small phase-slowness, where the eigenfunction penetrates the half space as is expected at the low-frequency limit. From left to right the panels are arranged along the continuous dispersion curve to gradually increasing phase-slowness. The rightmost diagram shows eigenfunctions completely confined to the layer, as is expected at the high-frequency limit. The shape of the eigenfunction varies smoothly along the dispersion curve and does not change in character, i. e. the number of zero-crossings does not change. The multi-valued section does not appear peculiar in any respect.

5 PROPAGATING WAVE-TRAIN

The roots of the secular equation (1) just indicate that eigensolutions of the boundary value problem exist at the respective pairs of frequency f and phase-slowness p. The normal modes can exist without explicit excitation and may propagate with phase velocity $c = p^{-1}$ in either direction as is indicated by the symmetry of $\Delta_{\mathrm{R}}(f,p)$ shown in Fig. 1. However, would waves of frequency f and phase-slowness p all along the multi-valued section of the dispersion curve be excited by an actual seismic source? How would the propagating wave field then look like? How do waves in the region of 'negative group-velocity' and 'zero group-velocity' appear in actual seismograms?

We use the reflectivity method (Fuchs & Müller 1971; Müller 1985) as implemented by Ungerer (Ungerer & Forbriger 2017; Ungerer & Wielandt 2017) to compute full wave forms for a given seismic source and a given component of surface displacement. When restricting the wave field to the multi-valued section of the dispersion relation, signals will be quite narrow-band, and seismograms will keep on oscillating with a single dominating frequency for a longer time. To allow us to study the propagation of transient wave groups, confined by a clear envelope, bandwidth shall be as large as possible. We therefore choose a model of a layer with a fixed bottom (*LFB*) where the multi-valuedness develops over the largest frequency interval for $\nu = \sqrt{7/16} = 0.4375$ (Malischewsky *et al.* 2017, Fig. 2). For the computation of synthetic seismograms, we approximate the rigid bottom by an impedance contrast of 100 between layer and half-space (Table 2). This is necessary, because the available implementation of the reflectivity method (Ungerer 1990) implicitly uses a homogeneous, elastic lower half-space.

As source we choose an explosion in 3 m depth, which excites the fundamental mode with smaller amplitude than a source at the surface would do. Fig. 5 and 9 display the modulus of Fourier-Bessel expansion coefficients (see appendix A) for the vertical and radial component of surface displacement, respectively. Like in Fig. 4 normal mode dispersion becomes visible by large magnitude of the coefficients. This is because the characteristic function appears in the denominator of the expression for the Fourier-Bessel expansion coefficients as pointed out by Kennett and Kerry (1979, section 5.4) and Müller (1985, eqs. 83 and 86). The dispersion-relation for the first overtone is multi-valued between 64 Hz and 74 Hz, approximately. Because the asymptotic phase-slowness at small frequency is $0\,\mathrm{s\,km^{-1}}$ in the case of *LFB* there exist only two valid, finite values of phase slowness at each frequency. The amplitude minimum of the vertical component at $(68\,\mathrm{Hz}, 0.4\,\mathrm{s\,km^{-1}})$ is due to the ellipticity of the mode at the surface turning into linear radial polarization. The minimum does not exist in the radial component. The expansion coefficients for the radial component (Fig. 9) demonstrate that the excited wave field contains contributions from throughout the multi-valued section with all values of phase-slowness for which normal modes may exist.

Table 2. Model *LFB* (layer with fixed bottom). The rigid bottom of the layer in this case is simulated by a ratio of 100 for seismic waves in the layer and the half-space. This is necessary, because the used implementation of the reflectivity method implicitly uses a homogeneous lower half-space. j: layer index, z_j: depth to bottom of layer, $v_{\mathrm{P}j}$, $v_{\mathrm{S}j}$: velocity of compressional and shear waves, ν_j: Poisson's ratio, ρ_j: mass density. $j = 2$ for the elastic half-space which approximates the rigid bottom. To provide anelastic dissipation in the computation of Fourier-Bessel expansion coefficients quality is set to $Q_{\mathrm{P}} = Q_{\mathrm{S}} = 200$.

j	z_j/m	$v_{\mathrm{P}j}/\mathrm{m\,s^{-1}}$	$v_{\mathrm{S}j}/\mathrm{m\,s^{-1}}$	ν_j	$\rho_j/\mathrm{kg\,m^{-3}}$
1	10	3000	1000	0.4375	1600
2	∞	300000	100000	0.4375	1600

5.1 Synthetic seismograms

5.1.1 Full wave field

The complete wave field for the vertical component of displacement is displayed in Fig. 10 in terms of a seismogram section. In comparison with signals on conventional structures the wave field is extraordinarily rich for *LFB*. Because the structure represents a wave guide with rigid bottom, all seismic energy is confined to the layer, the range of phase velocity approaches infinity (reverberating waves of vertical incidence). Nevertheless, two parts of the wave train can be distinguished. They are separated by the arrival time of the direct S-wave $t = r/v_{\mathrm{S}1} = r \cdot 1\,\mathrm{s\,km^{-1}}$, where r is offset. The slower wave group represents the fundamental mode signal. The earlier group mainly is composed of the higher mode signals. Both are rich in interference of waves with different phase velocity. Some waves propagate at phase velocity of $3\,\mathrm{km\,s^{-1}}$, the velocity of the direct P-wave. No clear first arrival of a refracted wave is apparent, because this does not exist in the *LFB* model.

5.1.2 Wave field section of 'negative group-velocity'

The wave-number integration approach of the reflectivity method allows us to compute a selected subsection of the wave field. We choose the section of apparently 'negative group-velocity' which is displayed in the upper inset of Fig. 5. This produces seismograms which allow us to study the features of the selected section in isolation. We emphasize that this wave train would not be observable, because the given seismic source would always excite all modes at once. Fig. 11 displays the resulting wave train for the full time and offset range (upper figure) as well as a section of the far field only (lower section). Obviously the wave train propagates with positive group slowness (with respect to the source, as discussed in section 4.1 above). This is consistent with the concept of energy emerging from the source. At the same time phase slowness is negative (Fig. 11, lower figure) and such has the opposite sign with respect to group slowness, which as well is consistent with the above made considerations. Phase slowness approximately is $p = -0.14\,\mathrm{s\,km^{-1}}$, which appears at about $f \approx 66\,\mathrm{Hz}$ in the dispersion relation (Fig. 5). This matches the dominating frequency in the wave train. Consider the symmetry with respect to $p = 0$

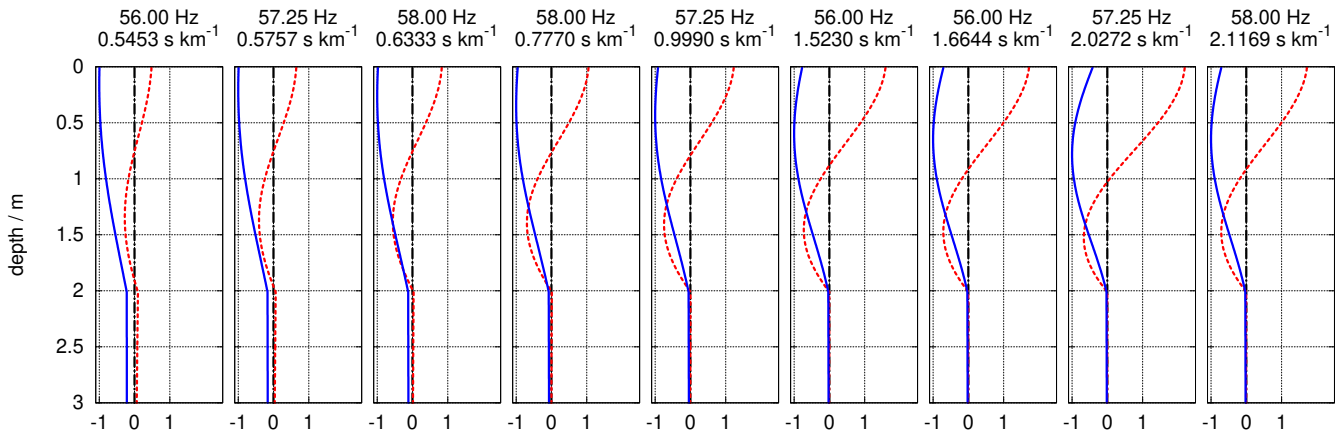

Figure 7. Displacement eigenfunctions for the first higher Rayleigh mode of structure *LOH* (Table 1). blue solid: vertical component. red dashed: horizontal component. Displayed amplitudes are normalized to the maximum of the vertical displacement and hence are charted without dimension. Eigenfunctions in the frequency interval between 56 Hz and 58 Hz are displayed, where the dispersion relation (Fig. 3) is multi-valued. The variation of eigenfunctions along the dispersion curve is quite ordinary, with displacement penetrating into the half-space at small frequency and displacement being confined to the layer at large frequency. No additional zero-crossing or other conspicuous feature indicates the unusual nature of the dispersion relation.

like exemplified in Fig. 1. Although only positive values of phase slowness are charted in Fig. 5, actually waves with negative phase slowness are excited in this section when referring the origin of the coordinate system to the seismic source. The ability to compose waves which are traveling with a negative phase-velocity, although parameter p the Fourier-Bessel coefficients is positive in a finite bandwidth, is a surprising but known property of the Bessel expansion (Forbriger 2003a, Fig. 6). We discuss this in appendix A. Group slowness approximately is $p_{\rm gr} \approx 0.15\,{\rm s\,km^{-1}}$. Both, group- and phase-slowness, are consistent with respect to eq. (B.14) and the gradient at 66 Hz, which is

$$\frac{{\rm d}\,p(f)}{{\rm d}\,f} \approx \frac{0.26\,{\rm s\,km^{-1}}}{10\,{\rm Hz}} \tag{3}$$

and positive because of $p(f) < 0$, such that group-slowness estimated on the basis of stationary phase would be

$$p_{\rm gr} \approx -0.14\,{\rm s\,km^{-1}} + 66\,{\rm Hz}\,\frac{0.26\,{\rm s\,km^{-1}}}{10\,{\rm Hz}} = 0.16\,{\rm s\,km^{-1}}. \tag{4}$$

This is consistent with Fig. 11 (upper figure).

5.1.3 Wave field section of 'zero group-velocity'

Similarly we investigate the wave field properties of the section where the gradient of the dispersion relation with respect to frequency becomes infinite, i. e. the section of 'zero group-velocity'. The Fourier-Bessel coefficients which capture the wave field of this section are displayed in the lower inset of Fig. 5. The bandwidth of the signal is even smaller than for the case of 'negative group-slowness'. Consequently the wave train appears quite monochromatic with a long lasting oscillation (upper section in Fig. 12). The far field (lower section in Fig. 12) appears like a standing wave composed by interference of two waves propagating in opposite direction where both have similar amplitude and the same frequency of about $f \approx 63\,{\rm Hz}$. The wavelength is about $\lambda \approx 54\,{\rm m}$, which corresponds to phase slowness of $p = f^{-1}\,\lambda^{-1} \approx 0.29\,{\rm s\,km^{-1}}$. This is consistent with the location of the point where the vertical tangent touches the dispersion relation as indicated in the lower inset of Fig. 5.

Wave groups only propagate slowly if time is smaller than 0.4 s and actually do not propagate at larger time (upper section in Fig. 12). Signals of largest amplitude as well as signals of smallest amplitude remain at the same location if time is larger. This is consistent with the conception of 'zero group-velocity'.

Like in the previous section, we emphasize that the wave train displayed in Fig. 12 would not be observable, because the given seismic source would always excite all modes at once.

5.2 Slant stack analysis fails

We use the synthetic wave form to test whether methods of wavefield transformation are able to capture the multi-valued section of the dispersion relation. We compute complete vertical component seismograms for an explosion in 3 m depth on the *LFB*-structure (Table 2). Seismograms are computed for a time window of 6.6 s with a sampling interval of about 0.81 ms at 100 offset values with a receiver interval of 5 m and a maximum offset of 500 m. The essential part of the wave train is displayed in Fig. 10 (with smaller receiver interval there).

We apply a Fourier-Bessel transformation as well as a slant-stack analysis (Forbriger 2003a). The first is most appropriate for wave trains emerging with cylindrical symmetry from a point source. It provides Fourier-Bessel expansion coefficients which reproduce the original wave train. The slant-stack uses a plane wave concept and in practice is primarily used to determine the dispersion of the Rayleigh waves through the location of amplitude maxima (McMechan & Yedlin 1981; Gabriels *et al.* 1987, e. g.). In case of the slant-stack we scale the wave form to offset independent amplitude. For both types of transformation a 20 per cent offset domain cosine taper is applied at the distant end of the profile. Figs. 13 and 14 show the results of Fourier-Bessel transformation and slant-stack, respectively.

The Fourier-Bessel transform (Fig. 13) essentially captures the complete wave field. The analysis is necessarily imperfect due to limited resolution and side-lobes caused by the finite length of profile and due a fragment of aliased signal at frequency larger than 90 Hz and slowness larger than $1\,{\rm s\,km^{-1}}$ which results from the finite receiver interval. Forbriger (2003a, sec. 2.2) discusses these

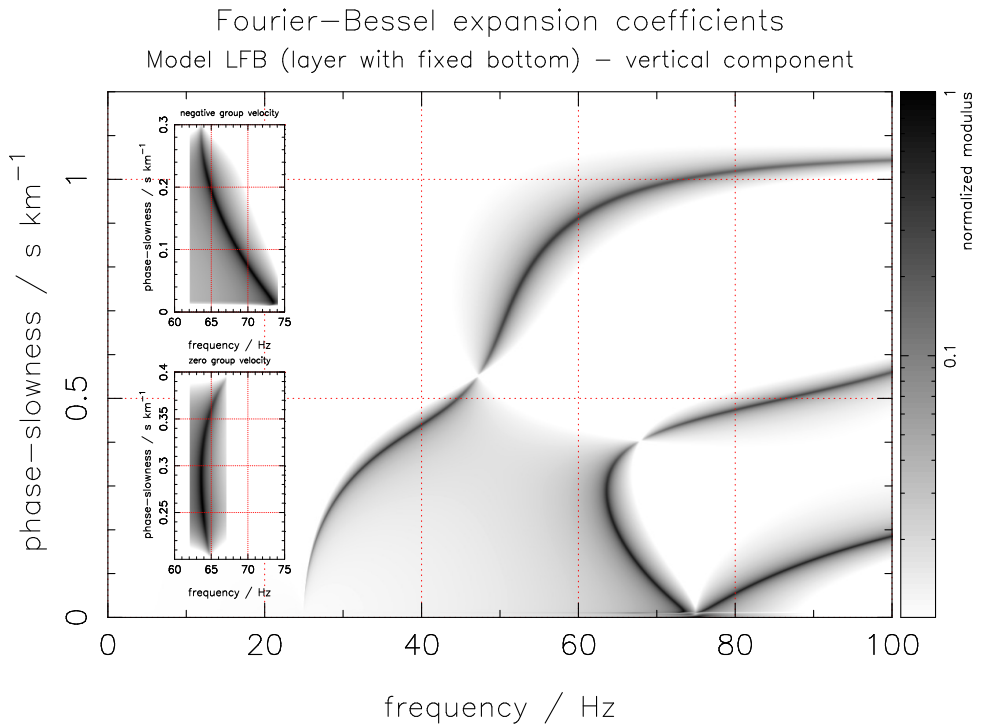

Figure 8. Modulus of Fourier-Bessel expansion coefficients for vertical displacement of the surface as excited by an explosion in 3 m depth in the structure *LFB* (Table 2). See appendix A for a definition of the expansion coefficients. For *LFB* with $\nu = \sqrt{7/16} = 0.4375$ the largest frequency interval of multi-valuedness is observed for the dispersion relation of the first higher mode. The smaller inset diagrams display subsets of the expansion coefficients which are obtained by application of tapers. The upper inset displays the section of apparently 'negative group-velocity', the lower inset displays the section of apparently 'zero group-velocity'.

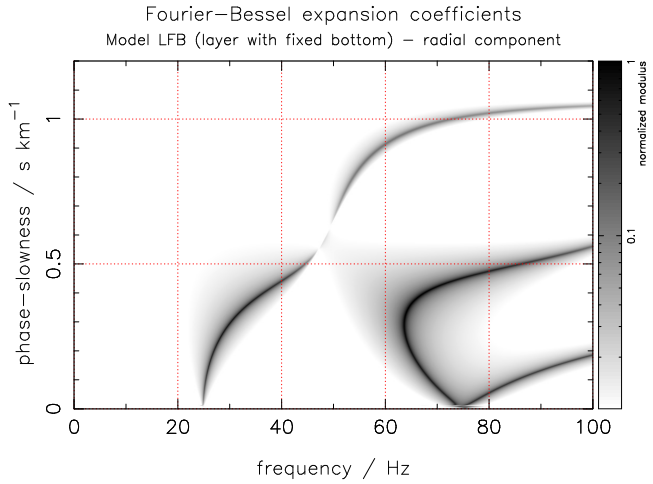

Figure 9. Modulus of Fourier-Bessel expansion coefficients for radial displacement of the surface as excited by an explosion in 3 m depth in the structure *LFB* (Table 2). See appendix A for a definition of the expansion coefficients. For *LFB* with $\nu = \sqrt{7/16} = 0.4375$ the largest frequency interval of multi-valuedness is observed for the dispersion relation of the first higher mode. The first overtone of the radial displacement is excited to finite amplitude throughout the multi-valued section of the dispersion relation in the frequency band between 64 Hz and 74 Hz.

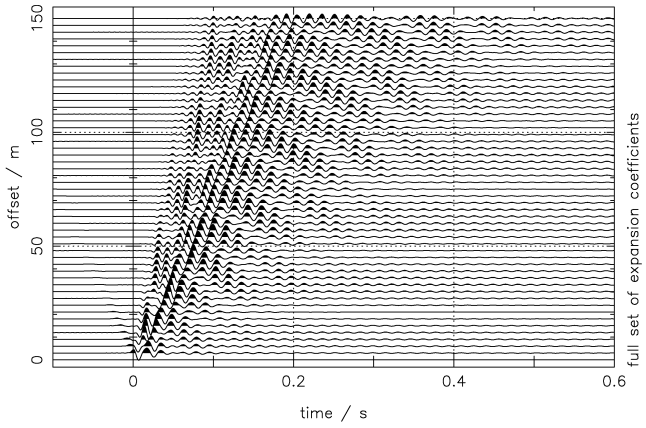

Figure 10. Vertical component seismograms computed for an explosion in 3 m depth in the structure *LFB* (Table 2). Fourier-Bessel expansion coefficients up to 150 Hz and 1.6 s km^{-1} (with a 30 per cent cosine taper at the upper limit of integration) are used. A fourth order Butterworth low-pass at 80 Hz is applied to the signals. Amplitudes are scaled by $(r/1\,\mathrm{m})^{0.8}$ to partly compensate for geometric spreading and dissipation, where r is offset. As is common in results of wave-number integration, truncation artifacts are apparent at small offset. They are due to the finite upper limit of numerical integration, similar to the Gibbs-Wilbraham phenomenon of Fourier series. In this case a signal propagating with negative phase slowness of about 1.5 s km^{-1} is apparent near the source at negative times. It quickly decays with offset. The artifact can reliably be distinguished from true wave-field properties, by its phase slowness depending on the upper limit of integration.

limitations of wave field transformation. Nevertheless the signal of the first overtone is completely reproduced in the frequency band of multi-valued dispersion.

However, the slant-stack is not able to capture the signal of the first overtone in this region (Fig. 14). Apparently this is caused by the seismograms having negative phase-slowness, while the slant-stack procedure can only capture signals of positive phase-slowness. Forbriger (2003a, sec. 5.1) discusses this with respect to the traveling wave properties of the Hankel functions of the first and second kind and refers to the slant-stack analysis. In consequence a multi-valued dispersion relation, if present in observed or synthetic seismograms, very likely would be missed by conventional techniques of dispersion analysis.

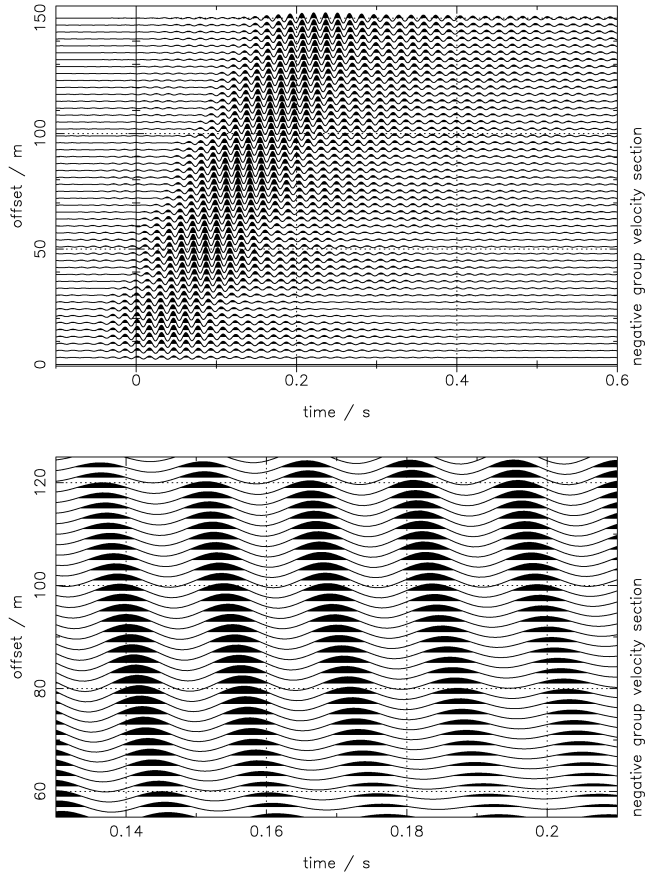

Figure 11. Wave train computed from the Fourier-Bessel expansion coefficients of the section of 'negative group-velocity' only. This section of expansion coefficients is displayed in the upper inset of Fig. 5. Amplitudes are scaled by $(r/1\,\mathrm{m})^{0.8}$ to partly compensate for geometric spreading and dissipation, where r is offset. The upper seismogram section displays the full time and offset range. Obviously the group velocity is positive with respect to source location and group-slowness is about $p_{\mathrm{gr}} \approx 0.15\,\mathrm{s\,km^{-1}}$. The lower seismogram section displays a section of the far field. Obviously, group and phase slowness have opposite sign, where phase slowness is about $p \approx -0.14\,\mathrm{s\,km^{-1}}$.

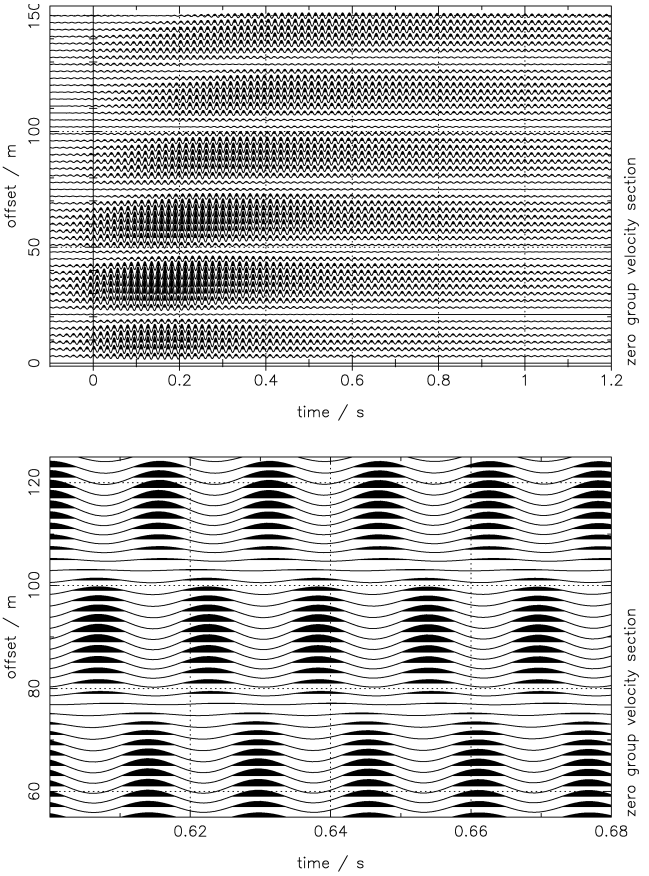

Figure 12. Wave train computed from the Fourier-Bessel expansion coefficients of the section of 'zero phase-velocity' only. This section of expansion coefficients is displayed in the lower inset of Fig. 5. Amplitudes are scaled by $(r/1\,\mathrm{m})^{0.8}$ to partly compensate for geometric spreading and dissipation, where r is offset. The upper seismogram section displays the full time and offset range. Time range is larger than in Fig. 10 and Fig. 11 because the signal is very narrow-band and therefore sustains for a larger time. The lower seismogram section displays a section of the far field. This pattern of the wave train is that of a standing wave composed through interference of waves propagating in opposite direction with the same phase velocity and amplitude. Nodes appear in intervals of 27 m. The wave length thus is $\lambda = 54\,\mathrm{m}$. Up to 70 m offset the group propagation is not obvious or does not take place at all, which is consistent with the notion of 'zero group-velocity'.

6 PAVEMENT STRUCTURES

6.1 Multi-valued dispersion of the fundamental mode

In the model which is defined in Table 3, we add a second layer with larger velocity on top. This is similar to a pavement structure which occasionally is investigated in civil engineering using Rayleigh waves (Ryden & Lowe 2004, e. g.). The stiff layer on top of the structure is similar to a plate. Consequently we observe a multi-valued dispersion curve for the fundamental mode in this case, as is shown in Fig. 15.

6.2 Frequency as a function of wave number

Remarkably, the inverse relation $f(p)$ for the fundamental mode becomes multi-valued too for this structure. The same would be observed for $f(c) = f(p^{-1})$. However $f(k)$ is single-valued, because $k = 2\pi f p$ increases sufficiently rapid with frequency f such that values of k do not appear twice along the curve. Similarly the curves of frequency as a function of wave number as presented by Lysmer (1970, Figure 5) as well as phase velocity as a function of

Table 3. Model *PAV* (pavement). Seismic parameters are chosen such that they could be realistic for pavement structures. A thin, stiff layer (pavement) is on top of a weaker layer (unconsolidated sediments) on top of a half-space (bedrock). Pavement and bedrock have a conventional value of Poisson's ratio near $\nu = 0.25$, while $\nu = \sqrt{7/16} = 0.4375$ in the layer of unconsolidated sediments, which can be due to partial saturation with water. j: layer index, z_j: depth to bottom of layer, $v_{\mathrm{P}j}$, $v_{\mathrm{S}j}$: velocity of compressional and shear waves, ν_j: Poisson's ratio, ρ_j: mass density. $j = 3$ for the elastic half-space.

j	z_j/m	$v_{\mathrm{P}j}$/m s^{-1}	$v_{\mathrm{S}j}$/m s^{-1}	ν_j	ρ_j/kg m^{-3}
1	0.20	4000.0	2310.0	0.2498	2600
2	2.00	532.8	177.6	0.4375	1800
3	∞	4000.0	2310.0	0.2498	2600

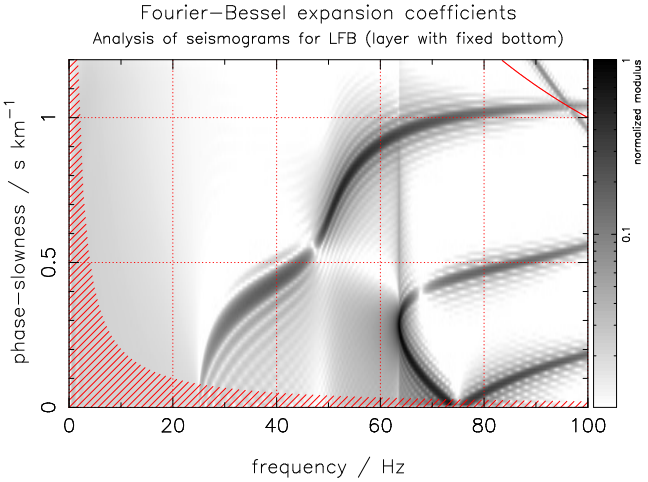

Figure 13. Modulus of the Fourier-Bessel transform of the complete seismograms computed for structure *LFB* (Table 2). Apart from the usual artifacts of discrete transformation (limited resolution, side-lobes, aliasing) the full signal is captured. This is obvious in comparison with the Fourier-Bessel expansion coefficients in Fig. 5. The hatched area indicates the resolution that can be obtained with a profile of 500 m length. Aliasing appears where the red hyperbola in the upper right hand corner intersects the signal.

wave number (Lysmer 1970, Figure 6) define single-valued relations.

This might raise the question for the 'natural' set of dependent and independent parameters. In shallow seismics dispersion commonly is expressed by $p(f)$ or $c(f)$, because we are used to apply a Fourier transformation to recorded data as a first step of spectral analysis and discuss solutions in terms of propagating waves. Whereas in global normal mode seismology dispersion commonly is expressed by $f(l)$, where l is the degree of the spherical harmonic, which relates to wave number $k = \sqrt{l\,(l+1)}$ (Dahlen & Tromp 1998, eq. 12.40). The latter choice is made, because on a

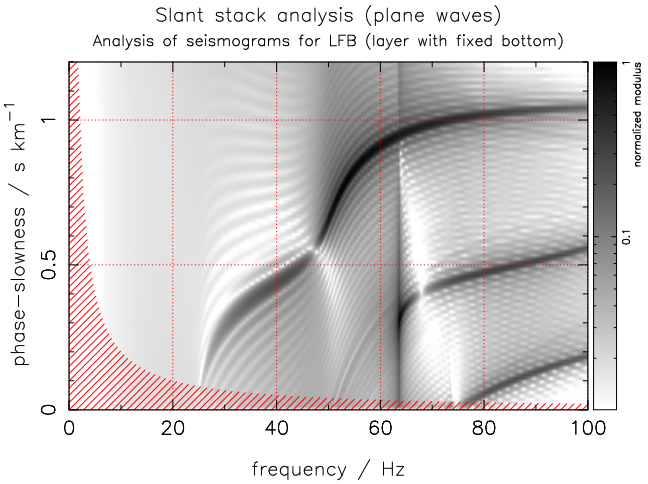

Figure 14. Slant-stack analysis of the complete seismograms computed for structure *LFB* (Table 2). Other than the Fourier-Bessel transformation (Fig. 13) the slant-stack misses the signal component of negative phase-velocity. This is obvious in comparison with the Fourier-Bessel expansion coefficients in Fig. 5. A part of the first higher Rayleigh-mode is missing between 64 Hz and 74 Hz at phase slowness smaller than 0.35 s km^{-1}. The hatched area indicates the resolution that can be obtained with a profile of 500 m length.

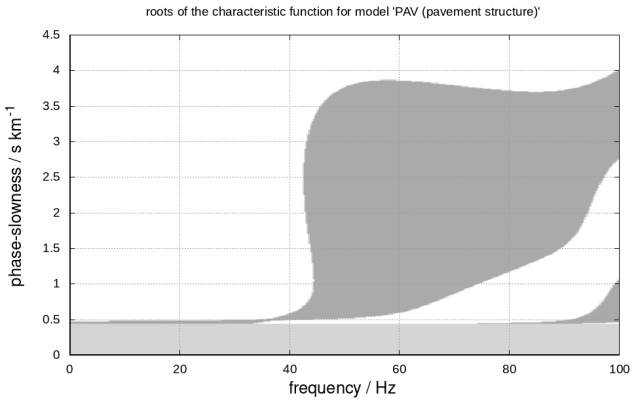

Figure 15. Sign of the characteristic function $\Delta_{\mathrm{R}}(f,p)$ for model *PAV* (Table 3). Grey and white areas have opposite sign. The characteristic function $\Delta_{\mathrm{R}}(f,p) = 0$ is satisfied along the lines where areas of different colors touch. Normal modes do not exist in the light-gray area at phase slowness $p < v^{-1}_{\mathrm{S,halfspace}}$, because energy would be radiated into the half-space. It is obvious that the relations $p(f)$ and $f(p)$ both are multi-valued for the fundamental mode.

sphere wave number is quantized naturally due to symmetry which results in a discrete set of l. For each l the mode's eigenfrequency f_l then has to be searched.

7 CONCLUSIONS

Rayleigh wave dispersion relations for simple, realistic structures can be multi-valued. There can exist more than one value of phase slowness $p(f)$, wave number $k(f)$, and phase velocity $c(f)$ at a given frequency f. The strength of the phenomenon depends on Poisson's ratio and velocity contrast between layers. Physical properties of the waves, like the variation of amplitude with depth or the propagation of wave groups, appear inconspicuous. The multi-valuedness appears to be due to the chosen mathematical decomposition (Fourier expansion and decomposition by phase-velocity) rather than due to an odd kind of seismic waves.

Traditional 'root-followers' inherently miss the multi-valued section of the dispersion relation. Deconvolution techniques and slant-stack analysis fail as well in such cases. Fourier phase of a single mode becomes meaningless. For pavement structures the fundamental mode can be multi-valued. At least in shallow seismic studies the applied algorithms must account for a possible multi-valuedness of Rayleigh wave dispersion in order to avoid false results. The Fourier-Bessel transformation (Forbriger 2003a) still provides reliable results in the case of multi-valued dispersion. Subsurface structure then can be inferred by inversion of the Fourier-Bessel expansion coefficients (Forbriger 2003b). Alternatively a dispersion curve read manually from the coefficients can be inverted to subsurface structure with the method proposed by Maraschini *et al.* (2010) which directly uses the characteristic function to setup the objective function and does not require to locate roots.

ACKNOWLEDGMENTS

Walter Zürn contributed very helpful comments on the manuscript. The editor, Herve Chauris, and two anonymous reviewers provided encouraging and helpful comments. We are grateful to Wolfgang

Friederich for sharing his code `flspher` with us. Robert Hermann provides `sdisp96` for public download (Herrmann 2018). Similarly `geopsy` is available for download (Geopsy team 2017). Peter Malischewsky was supported by the Deutsche Forschungsgemeinschaft (DFG) under grant FO506/1-1.

Author's contributions: All authors contributed their considerations to the study and comments to the manuscript. MO contributed the computation of synthetic dispersion relations with programs `geopsy` and `sdisp96`. YP provided a complete computation of dispersion curves, capturing the multi-valued section. LG computed eigenfunctions. TF and PM initiated this contribution with findings from an earlier study. TF designed the concept of this study, provided synthetic seismograms, characteristic function sign patterns, and synthetic dispersion curves with `flspher`, and drafted the manuscript.

This paper has been produced using the Blackwell Scientific Publications GJI LaTeX2e class file.

REFERENCES

Aki, K. & Richards, P. G., 2002. *Quantitative Seismology*. University Science Books, Sausalito, 2nd edn.

Buchen, P. & Ben-Hador, R., 1996. Free-mode surface-wave computations, *Geophys. J. Int.*, **124**, 869–887. doi: 10.1111/j.1365-246X.1996.tb05642.x.

Carcione, J. M., Gei, D. & Treitel, S., 2010. The velocity of energy through a dissipative medium, *Geophysics*, **75**(2), T37–T47. doi: 10.1190/1.3346064.

Cui, H., Lin, W., Zhang, H., Wang, X. & Trevelyan, J., 2016. Backward waves with double zero-group-velocity points in a liquid-filled pipe, *J. Acoust. Soc. Am.*, **139**(3), 1179–1194. doi: 10.1121/1.4944046.

Cès, M., Clorennec, D., Royer, D. & Prada, C., 2011. Thin layer thickness measurements by zero group velocity Lamb mode resonances, *Rev. Sci. Instrum.*, **82**(11), 114902. doi: 10.1063/1.3660182.

Dahlen, F. A. & Tromp, J., 1998. *Theoretical Global Seismology*. Princeton University Press, Princeton, New Jersey.

Every, A. G., 2002. Measurement of the near-surface elastic properties of solids and thin supported films, *Meas. Sci. Technol.*, **13**(5), R21–R39. doi: 10.1088/0957-0233/13/5/201.

Forbriger, T., 2003a. Inversion of shallow-seismic wavefields: I. Wavefield transformation, *Geophys. J. Int.*, **153**, 719–734. doi: 10.1046/j.1365-246X.2003.01929.x.

Forbriger, T., 2003b. Inversion of shallow-seismic wavefields: II. Inferring subsurface properties from wavefield transforms, *Geophys. J. Int.*, **153**, 735–752. doi: 10.1046/j.1365-246X.2003.01985.x.

Forbriger, T., Groos, L. & Schäfer, M., 2014. Line-source simulation for shallow-seismic data. part 1: theoretical background, *Geophys. J. Int.*, **198**, 1387–1404. doi: 10.1093/gji/ggu199.

Foti, S., Hollender, F., Garofalo, F., Albarello, D., Asten, M., Bard, P.-Y., Comina, C., Cornou, C., Cox, B., Di Giulio, G., Forbriger, T., Hayashi, K., Lunedei, E., Martin, A., Mercerat, D., Ohrnberger, M., Poggi, V., Renalier, F., Sicilia, D. & Socco, V., 2018. Guidelines for the good practice of surface wave analysis: a product of the InterPACIFIC project, *B. Earthq. Eng.*, **16**(6), 2367–2420. doi: 10.1007/s10518-017-0206-7.

Friederich, W., 1999. Propagation of seismic shear and surface waves in a laterally heterogeneous mantle by multiple forward scattering, *Geophys. J. Int.*, **136**, 180–204. doi: 10.1046/j.1365-246X.1999.00720.x.

Friederich, W. & Dalkolmo, J., 1995. Complete synthetic seismograms for a spherically symmetric earth by a numerical computation of the Green's function in the frequency domain, *Geophys. J. Int.*, **122**, 537–550. doi: 10.1111/j.1365-246X.1995.tb07012.x.

Fuchs, K. & Müller, G., 1971. Computation of synthetic seismograms with the reflectivity method and comparison with observations, *Geophys. J. R. astr. Soc.*, **23**(4), 417–433. doi: 10.1111/j.1365-246X.1971.tb01834.x.

Gabriels, P., Snieder, R. & Nolet, G., 1987. In situ measurements of shear-wave velocity in sediments with higher-mode Rayleigh waves, *Geophys. Prospect.*, **35**, 187–196. doi: 10.1111/j.1365-2478.1987.tb00812.x.

Geopsy team, 2017. geopsy. Open source software. http://geopsy.org/ (last accessed: 2017-02-09).

Herrin, E. & Goforth, T., 1977. Phase-matched filters: Application to the study of Rayleigh waves, *Bull. Seism. Soc. Am.*, **67**(5), 1259–1275.

Herrmann, R. B., 2013. Computer programs in seismology: An evolving tool for instruction and research, *Seism. Res. Lett.*, **84**(6), 1081–1088. doi: 10.1785/0220110096.

Herrmann, R. B., 2018. Computer programs in seismology. Open source software. http://www.eas.slu.edu/eqc/eqccps.html (last accessed: 2018-08-22).

Kausel, E., 2012. Number and location of zero-group-velocity modes, *J. Acoust. Soc. Am.*, **131**(5), 3601–3610. doi: 10.1121/1.3695398.

Kausel, E., Malischewsky, P. & Barbosa, J., 2015. Osculations of spectral lines in a layered medium, *Wave Motion*, **56**, 22–42. doi: 10.1016/j.wavemoti.2015.01.004.

Kennett, B. L. N. & Kerry, N. J., 1979. Seismic waves in a stratified half space, *Geophys. J. Int.*, **57**(3), 557–583. doi: 10.1111/j.1365-246X.1979.tb06779.x.

Kovach, R. L., 1978. Seismic surface waves and crustal and upper mantle structure, *Rev. Geophys. Space Phys.*, **16**(1), 1–13. doi: 10.1029/RG016i001p00001.

Kästle, E. D., El-Sharkawy, A., Boschi, L., Meier, T., Rosenberg, C., Bellahsen, N., Cristiano, L. & Weidle, C., 2018. Surface wave tomography of the Alps using ambient-noise and earthquake phase velocity measurements, *J. Geophys. Res.: Solid Earth*, **123**(2), 1770–1792. doi: 10.1002/2017JB014698.

Lamb, H., 1904. On group-velocity, *Proc. Lond. Math. Soc.*, **s2-1**(1), 473–479. doi: 10.1112/plms/s2-1.1.473.

Lamb, H., 1917. On waves in an elastic plate, *Proc. Roy. Soc. London A*, **93**(648), 114–128. doi: 10.1098/rspa.1917.0008.

Lysmer, J., 1970. Lumped mass method for Rayleigh waves, *Bull. Seism. Soc. Am.*, **60**(1), 89–104.

Malischewsky, P. G. & Forbriger, T., 2020. May Rayleigh waves propagate with group- and phase-velocities of opposite sign in the valley of Mexico City?, *Geofisica Internacional*, **59**(2), in print.

Malischewsky, P. G., Forbriger, T. & Lomnitz, C., 2017. Unusual, equivocal Rayleigh-dispersion curves for simple models taking into account the special propagation conditions in the valley of Mexico City (CDMX) — preliminary results, *Geofisica Internacional*, **56**(1), 7–12. doi: 10.19155/geofint.2017.056.1.1.

Maraschini, M., Ernst, F., Foti, S. & Socco, L. V., 2010. A new misfit function for multimodal inversion of surface waves, *Geophysics*, **75**(4), G31–G43. doi: 10.1190/1.3436539.

Maznev, A. A. & Every, A. G., 2009. Surface acoustic waves with negative group velocity in a thin film structure on silicon, *Appl. Phys. Lett.*, **95**(1), 011903. doi: 10.1063/1.3168509.

Maznev, A. A. & Every, A. G., 2011. Existence of backward propagating acoustic waves in supported layers, *Wave Motion*, **48**(5), 401–407. doi: 10.1016/j.wavemoti.2011.02.002.

McMechan, G. A. & Yedlin, M. J., 1981. Analysis of dispersive waves by wave field transformation, *Geophysics*, **46**, 869–874. doi: 10.1190/1.1441225.

Müller, G., 1985. The reflectivity method: A tutorial, *J. Geophys.*, **58**, 153–174. http://resolver.sub.uni-goettingen.de/purl?PPN1015067948_0058.

Negishi, K., 1987. Existence of negative group velocities in Lamb waves, *Jpn. J. Appl. Phys.*, **26**(S1), 171–173. doi: 10.7567/JJAPS.26S1.171.

Nishimiya, K., Yamamoto, K., Mizutani, K. & Wakatsuki, N., 2007. Negative group velocities of Lamb-type waves in a glass/water/glass structure controlled by the thickness of water layer, *Jpn. J. Appl. Phys.*, **46**(7B), 4483–4485. doi: 10.1143/jjap.46.4483.

Oulton, R. F. & Pendry, J. B., 2013. Negative refraction imaging through the looking-glass, *Nature Physics*, **9**(6), 323–324. doi: 10.1038/nphys2645.

Pendry, J. B., 2009. Negative refraction (reprinted from contemporary physics, vol 45, pg 191), *Contemp. Phys.*, **50**(1), 363–374. doi:

10.1080/00107510902734771.

Russell, D. R., Herrmann, R. B. & Hwang, H.-J., 1988. Application of frequency variable filters to surface-wave amplitude analysis, *Bull. Seism. Soc. Am.*, **78**(1), 339–354.

Ryden, N. & Lowe, M. J. S., 2004. Guided wave propagation in three-layer pavement structures, *J. Acoust. Soc. Am.*, **116**(5), 2902–2913. doi: 10.1121/1.1808223.

Schwab, F. & Knopoff, L., 1972. Fast surface wave and free mode computations. In *Methods in Computational Physics, Seismology: Surface Waves and Earth Oscillations*, ed. B. A. Bolt, vol. 11, pp. 87–180. Academic Press, New York and London. doi: 10.1016/B978-0-12-460811-5.50008-8.

Socco, L. V., Foti, S. & Boiero, D., 2010. Surface-wave analysis for building near-surface velocity models - established approaches and new perspectives, *Geophysics*, **75**(5), A83–A102. doi: 10.1190/1.3479491.

Sommerfeld, A., 1949a. Chapter IV: Cylinder and sphere problems. In *Partial Differential Equations in Physics*, vol. 1 of *Pure and Applied Mathematics*, pp. 84–165. Elsevier. doi: 10.1016/S0079-8169(08)60770-9.

Sommerfeld, A., 1949b. Chapter VI: Problems of radio. In *Partial Differential Equations in Physics*, vol. 1 of *Pure and Applied Mathematics*, pp. 236–296. Elsevier. doi: 10.1016/S0079-8169(08)60772-2.

Sommerfeld, A., 1949c. *Lectures on theoretical physics*, vol. 6: Partial differential equations in physics of *Pure and applied mathematics; 1*. Academic Press, New York, 5th edn.

Sèbe, O., Forbriger, T. & Ritter, J. R. R., 2009. The shear wave velocity underneath Bucharest city, Romania, from the analysis of Love waves, *Geophys. J. Int.*, **176**(3), 965–979. doi: 10.1111/j.1365-246X.2008.04027.x.

Takeuchi, H. & Saito, M., 1972. Seismic surface waves. In *Methods in Computational Physics, Seismology: Surface Waves and Earth Oscillations*, ed. B. A. Bolt, vol. 11, pp. 217–295. Academic Press, New York and London. doi: 10.1016/B978-0-12-460811-5.50010-6.

Tamm, K., Peets, T., Engelbrecht, J. & Kartofelev, D., 2017. Negative group velocity in solids, *Wave Motion*, **71**, 127–138.

Tolstoy, I. & Usdin, E., 1957. Wave propagation in elastic plates: Low and high mode dispersion, *J. Acoust. Soc. Am.*, **29**, 37–42. doi: 10.1121/1.1908675.

Tuan, T. T., 2009. *The ellipticity (H/V-ratio) of Rayleigh surface waves*. Dissertation, Friedrich-Schiller University Jena, Germany. https://nbn-resolving.org/urn:nbn:de:gbv:27-20090306-134913-8 (last accessed: 2019-06-05).

Ungerer, J., 1990. *Berechnung von Nahfeldseismogrammen mit der Reflektivitätsmethode*. Diplomarbeit, Institut für Geophysik, Universität Stuttgart, Germany.

Ungerer, J. & Forbriger, T., 2017. Reflectivity method (refmet). Open source software. https://git.scc.kit.edu/Seitosh/Seitosh/tree/master/src/synt/ref/refmet (last accessed: 2017-02-09).

Ungerer, J. & Wielandt, E., 2017. Reflectivity method (refseis). Open source software. http://www.software-for-seismometry.de/software/refseis/ (last accessed: 2017-02-09).

Wang, R., 1999. A simple orthonormalization method for stable and efficient computation of Green's functions, *Bull. Seism. Soc. Am.*, **89**(3), 733–741. http://www.bssaonline.org/content/89/3/733 (last accessed: 2017-02-10).

Wathelet, M., 2008. An improved neighborhood algorithm: Parameter conditions and dynamic scaling, *Geophys. Res. Lett.*, **35**(9). doi: 10.1029/2008GL033256, L09301.

Wathelet, M., Jongmans, D. & Ohrnberger, M., 2004. Surface-wave inversion using a direct search algorithm and its application to ambient vibration measurements, *Near Surf. Geophys.*, **2**, 211–221. http://geopsy.org/ (last accessed: 2017-02-09).

Wielandt, E., 1992. Signalverarbeitung in der Geophysik. Lecture notes, University of Stuttgart, Germany.

Wolf, J., Ngoc, T. D. K., Kille, R. & Mayer, W. G., 1988. Investigation of Lamb waves having a negative group velocity, *J. Acoust. Soc. Am.*, **83**(1), 122–126. doi: 10.1121/1.396438.

Woodhouse, J. H., 1988. The calculation of eigenfrequencies and eigenfunctions of the free oscillations of the earth and the sun. In *Seismological Algorithms*, ed. D. J. Doornbos, chap. IV.2, pp. 321–370. Academic Press, London.

APPENDIX A: FOURIER-BESSEL EXPANSION

Fourier-Bessel expansion coefficients (Forbriger 2003a) are used by methods for the computation of synthetic seismograms, which make use of separation of variables and wave-number integration like the reflectivity method (Fuchs & Müller 1971; Müller 1985, e. g.) or others (Kennett & Kerry 1979; Wang 1999, e. g.). For a source with cylindrical symmetry, like a vertical force or an explosion, the vertical component ground displacement

$$u_z(t,r) = \int_{-\infty}^{+\infty} \tilde{u}_z(\omega,r)\, e^{-i\omega t} \frac{\mathrm{d}\,\omega}{2\pi} \tag{A.1}$$

is given as a Fourier expansion with Fourier transform $\tilde{u}_z(\omega,r)$ which itself is expressed by

$$\tilde{u}_z(\omega,r) = \int_{0}^{+\infty} G_z(\omega,p)\, J_0(\omega p r)\, p\ \mathrm{d}\,p. \tag{A.2}$$

Bessel functions $J_0(\omega p r)$ of the first kind and order zero are used in the kernel. The $G_z(\omega,p)$ are the Fourier-Bessel expansion coefficients of the vertical component of wave field. Likewise that radial component ground displacement

$$u_r(t,r) = \int_{-\infty}^{+\infty}\int_{0}^{+\infty} G_r(\omega,p)\, J_1(\omega p r)\, e^{-i\omega t}\, p\ \mathrm{d}\,p \frac{\mathrm{d}\,\omega}{2\pi} \tag{A.3}$$

is expressed by using Bessel functions $J_1(\omega p r)$ of first kind and order one in the kernel for a source with cylindrical symmetry.

The very same coefficients can be used for the expansion

$$u_{\mathrm{L}z}(t,r) = 2\int_{-\infty}^{+\infty}\int_{0}^{+\infty} G_z(\omega,p)\ \cos(\omega p r)\, e^{-i\omega t}\, \frac{\mathcal{C}}{\omega}\ \mathrm{d}\,p \frac{\mathrm{d}\,\omega}{2\pi}$$

and

$$u_{\mathrm{L}r}(t,r) = 2\int_{-\infty}^{+\infty}\int_{0}^{+\infty} G_r(\omega,p)\ \sin(\omega p r)\, e^{-i\omega t}\, \frac{\mathcal{C}}{\omega}\ \mathrm{d}\,p \frac{\mathrm{d}\,\omega}{2\pi}$$

of plane waves emerging from a line source, where $\mathcal{C}$ accounts for the different units of force density in the definition of the line source with respect to a point source (Forbriger *et al.* 2014, secs. 2.2 and 4).

All integration takes place over positive values of phase slowness p only. The kernel functions (Bessel functions of the first kind as well as the trigonometric sine and cosine functions) do not appear to represent traveling waves. How can these integral expansions then express traveling waves of either propagation direction? Sommerfeld (1949b; 1949c, §32) discusses this property of the Bessel expansion. In fact the Bessel function of the first kind

$$J_n(\omega p r) = \frac{1}{2}\left(H_n^{(1)}(\omega p r) + H_n^{(2)}(\omega p r)\right) \tag{A.4}$$

equals the sum of the Hankel functions of first and second kind (Sommerfeld 1949a, §19). In the far field the Hankel functions represent propagating waves in either direction. Both contributions (and hence the Bessel function of the first kind) are required in

the kernel of the expansion integral when expressing the source in the separation of variables. The expansion in fact is able to express propagating waves. Sommerfeld (1949b, §32) points out that with

$$\tilde{u}_z(\omega, r) = \int_0^{+\infty} G_z(\omega, p)\, J_0(\omega p r)\, p \, \mathrm{d}\, p \tag{A.5}$$

$$= \frac{1}{2} \int_{-\infty}^{+\infty} G_z(\omega, p)\, H_n^{(1)}(\omega p r)\, p \, \mathrm{d}\, p \tag{A.6}$$

$$= \frac{1}{2} \int_{-\infty}^{+\infty} G_z(\omega, p)\, H_n^{(2)}(\omega p r)\, p \, \mathrm{d}\, p \tag{A.7}$$

the expansion can be expressed by kernels which represent traveling waves in the far field if $G_z(\omega, p) = G_z(\omega, -p)$. Integration then takes place over the range of negative as well as positive values of phase slowness.

The direction of propagation is controlled by the variation of the Fourier phase with offset. Let

$$f(t) = \int_{-\infty}^{+\infty} \tilde{f}(\omega)\, e^{-i\omega t}\, \frac{\mathrm{d}\,\omega}{2\pi} \tag{A.8}$$

be the wave form of a propagating wavelet. Then the Fourier transform

$$\tilde{\phi}(x, \omega) = \tilde{f}(\omega)\, e^{i\omega p x} \tag{A.9}$$

defines a plane wave with a propagating wavelet

$$\phi(x, t) = f(px - t) = \int_{-\infty}^{+\infty} \tilde{\phi}(x, \omega)\, e^{-i\omega t}\, \frac{\mathrm{d}\,\omega}{2\pi} \tag{A.10}$$

of phase slowness p. Hence the direction of propagation is controlled by the sign of the phase factor in eq. (A.9).

The selection of waves of either direction of propagation in a Bessel expansion is controlled by the expansion coefficients. This is demonstrated by the so-called 'Sommerfeld integral' as used by Müller (1985, sec. 4.2, eqs. 58–61) and defined by Sommerfeld (1949b, §31.14). It expresses a propagating spherical wave

$$\frac{e^{i\omega p_0(\omega) r}}{r} = \int_0^{+\infty} \frac{1}{\sqrt{p^2 - p_0^2(\omega)}}\, J_0(\omega p r)\, \omega p \, \mathrm{d}\, p \tag{A.11}$$

by Bessel expansion. The wave propagates with phase slowness $p_0(\omega)$, where the direction of propagation is controlled by the Riemann sheet taken during integration. In eq. (A.11) the complex square root must be taken with positive real part.

APPENDIX B: PHASE- AND GROUP-VELOCITY

Let

$$\tilde{\phi}(x, \omega) = A(\omega)\, e^{ik(\omega)\, x} \tag{B.1}$$

be the Fourier transform of a plane wave

$$\phi(x, t) = \int_{-\infty}^{+\infty} \tilde{\phi}(x, \omega)\, e^{-i\omega t}\, \frac{\mathrm{d}\,\omega}{2\pi} \tag{B.2}$$

$$= \int_{-\infty}^{+\infty} A(\omega)\, e^{i\,\{k(\omega)\, x - \omega\, t\}}\, \frac{\mathrm{d}\,\omega}{2\pi}. \tag{B.3}$$

The wave propagates with wave number $k(\omega)$ at frequency ω. Based on this definition Lamb (1904) and Wielandt (1992) give very concise derivations of phase- and group-velocity.

To obtain phase velocity

$$c(\omega) = \frac{\mathrm{d}\, x(t)}{\mathrm{d}\, t} \tag{B.4}$$

$x(t)$ must be chosen such that the Fourier phase $k\, x(t) - \omega\, t$ in eq. (B.3) remains constant. The condition

$$\frac{\mathrm{d}}{\mathrm{d}\, t}\, (k\, x(t) - \omega\, t) = 0 \tag{B.5}$$

results in

$$c(\omega) = \frac{\mathrm{d}\, x(t)}{\mathrm{d}\, t} = \frac{\omega}{k}. \tag{B.6}$$

Phase slowness then is

$$p(\omega) = \frac{1}{c(\omega)} = \frac{k}{\omega}. \tag{B.7}$$

To obtain group velocity

$$v_{\mathrm{gr}} = \frac{\mathrm{d}\, x(t)}{\mathrm{d}\, t} \tag{B.8}$$

$x(t)$ must be chosen such that waves of similar frequency interfere constructively in eq. (B.3) and compose a wave group in the seismogram. This is expressed with the concept of stationary phase by the condition

$$\frac{\mathrm{d}}{\mathrm{d}\, \omega}\, (k\, x(t) - \omega t) = 0 \tag{B.9}$$

which results in

$$\frac{\mathrm{d}\, k}{\mathrm{d}\, \omega} x(t) = t \tag{B.10}$$

and

$$x(t) = t \frac{\mathrm{d}\, \omega}{\mathrm{d}\, k}. \tag{B.11}$$

Group velocity hence is

$$v_{\mathrm{gr}} = \frac{\mathrm{d}\, x(t)}{\mathrm{d}\, t} = \frac{\mathrm{d}\, \omega}{\mathrm{d}\, k} \tag{B.12}$$

and correspondingly group slowness

$$p_{\mathrm{gr}} = \frac{\mathrm{d}\, k}{\mathrm{d}\, \omega}. \tag{B.13}$$

Eq. (B.7) expresses wave-number dispersion $k(\omega) = \omega\, p(\omega)$ by phase-slowness dispersion. Using this in eq. (B.13) group-slowness dispersion

$$p_{\mathrm{gr}}(\omega) = p(\omega) + \omega\, \frac{\mathrm{d}\, p(\omega)}{\mathrm{d}\, \omega} \tag{B.14}$$

can be expressed by phase-slowness dispersion $p(\omega)$. Formally group slowness becomes negative with $p_{\mathrm{gr}}(\omega) < 0$ if

$$\frac{\mathrm{d}\, p(\omega)}{\mathrm{d}\, \omega} < -\frac{p}{\omega} \tag{B.15}$$

which is identical with

$$\frac{\mathrm{d}\, p(f)}{\mathrm{d}\, f} < -\frac{p}{f}. \tag{B.16}$$

If velocity is defined positive for propagation taking place with increasing distance to the source, it commonly turns out that actually $p_{\mathrm{gr}}(\omega)$ is positive and $p(\omega)$ is negative as is discussed in the text.

Similar expressions can be derived for phase velocity and group velocity. Group velocity vanishes for example, where the

derivative of phase velocity with respect to frequency becomes infinite. This is the case at the turning points of the dispersion curve at 56 Hz and 58 Hz in Fig. 3.

While wave number $k(\omega) = \omega\, p(\omega)$ (and thus also phase slowness $p(\omega)$) is a well defined quantity (eigenvalue) in normal mode theory, this is not the case for group slowness. The above sketched derivation of group slowness neglects the assumption for the behavior of the Fourier amplitude $A(\omega)$ in the application of the concept of stationary phase. Only for well behaved $A(\omega)$ which only smoothly varies with ω the above given results are reasonable in terms of propagating wave-groups.